pubs.acs.org/JACS

Tip-Patched Nanoprisms from Formation of Ligand Islands

Ahyoung Kim, ^{†,¶} Shan Zhou, ^{†,‡,¶}© Lehan Yao, [†] Stacey Ni, [†] Binbin Luo, [†] Charles E. Sing, ^{§,∥}© and Qian Chen*, ^{†,‡,∥,⊥}©

†Department of Materials Science and Engineering, ‡Materials Research Laboratory, [§]Department of Chemical and Biomolecular Urbana-Champaign, Urbana, Illinois 61801, United States Engineering, Beckman Institute for Advanced Science and Technology, and Department of Chemistry, University of Illinois at

Supporting Information

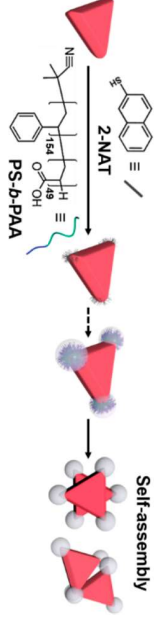
cluster as they adsorb, to preparing nanoparticles (NPs) with precisely sized surface patches. Using gold triangular nanoprisms and 2-naphthalenethiols (2-NAT) as a generalizable strategy to make patchy NPs of various shapes for emergent assemblies and applications. interactions. Langmuir adsorption. The tip-patched into unexpected twisted dimers due to consistent field theory modeling, from which we exclude Langmuir adsorption. The tip-patched prisms assemble shaped to a reuleaux triangle by increasing the 2-NAT-to-prism concentration ratio. This trend matches with microscopy imaging upon attaching polystyrene-b-poly-(acrylic acid). Using this method, the shape of patchy transmission electron microscopy and atomic force of tip patches. The patches are rendered visible for direct prototypical system, we show that the preferential adsorption of 2-NAT on the prism tips leads to formation established for planar ABSTRACT: We apply the concept of "island formation" (acrylic acid). Using this method, predictions of island formation as elucidated by our selfis varied from small lobed, big lobed, We expect the island formation as substrates, where ligands laterally the patch-patch trefoil, T-

surface patches, via a one-pot process, to realize the great potentials of patchy NPs in directed assembly, 5-7 catalysis, 8 and drug delivery. Such a ligand island formation method tetrahedral and octahedral NPs, 14 although further extension into temperature. 12 Indeed, alkanethiolate patches were found to form on gold nanospheres following the JMAK model, 13 postadsorption reorganization of uniformly coated polymer ligands on NPs upon a change in solvent polarity or islands. This mechanism, if applicable to nanoparticles (NPs) substrates, followed by lateral expansion of these sites Lo domains can be formed in self-assembled monolayers of thiolated molecules on planar gold substrates. 1-3 This process adsorption. although only with random patterns due to nonselective ligand differs from the prevailing synthesis of patchy NPs utilizing can pattern the NPs with precisely sized ligand islands, namely xtensive studies have shown where ligand adsorption sites nucleate on gold the Johnson-Mehl-Avrami-Kolmogorov (JMAK) Other proof-of-concept work suggested preferthat "island-like" ligand although not realizing edges Ħ.

for the first time to make patchy NPs with precise patch we implement the concept of ligand island formation

and shape. We use a combination of gold triangular nanoprisms and 2-naphthalenethiol (2-NAT) ligands as a prototypical system (Scheme 1). The gold prisms have planar

and Slanting Diamonds Ligand Island Formation and Their Self-Assembly into Stars Scheme 1. Preparation of Tip-Patched Nanoprisms via



island formation can serve as a general and potent method to pattern functional patches on NPs. and slanting patches lead to hitherto unachieved twisted assemblies The steric hindrance and electrostatic repulsion of PS-b-PAA attachment to the prism reinforces our hypothesis that ligand tron microscopy (TEM) imaging of the patch size and shape. Self-consistent field theory (SCFT) modeling of PS-b-PAA phobicity of 2-NAT allows polystyrene-b-poly(acrylic acid) (PS-b-PAA) to attach on the 2-NAT patches due to hydrophobic attraction,¹⁷ which facilitates transmission elecadsorption sites into islands of desired sizes. at the prism tips. The 2-NAT ligands have strong lateral $\pi - \pi$ attraction 15,16 to promote the expansion of the initial faces and curved tips, which allows selective ligand adsorption island formation dictates the controllable expansion of patches. diamonds, Scheme 1). We foresee that ligand The hydro-

are charged PAA block sticking outward onto the prism surface S1). During this one-pot process, the 2-NAT molecules adsorb dimethyl formamide/H₂O mixture at 110 °C for 2 h (Table Next, an aqueous suspension of the prisms with a controlled concentration is mixed with 2-NAT and PS-b-PAA in a As a mist unconstant, $\frac{1}{2}$ and $\frac{1}{2}$ are synthesized following literature methods. Is, $\frac{1}{2}$ and $\frac{1}{2}$ are synthesized following literature methods. As a redispersed in water and characterized by first demonstration, tip-patched prisms are robustly d in low dispersity. The parent gold prisms (side to the ф 2-NAT coated region and the negatively ck sticking outward. ^{20,21} The product prisms patches by gold-thiol bond, with PS-b-PAA are clearly seen

Published: Received: July 17, May 17, Journal of the American Chemical Society

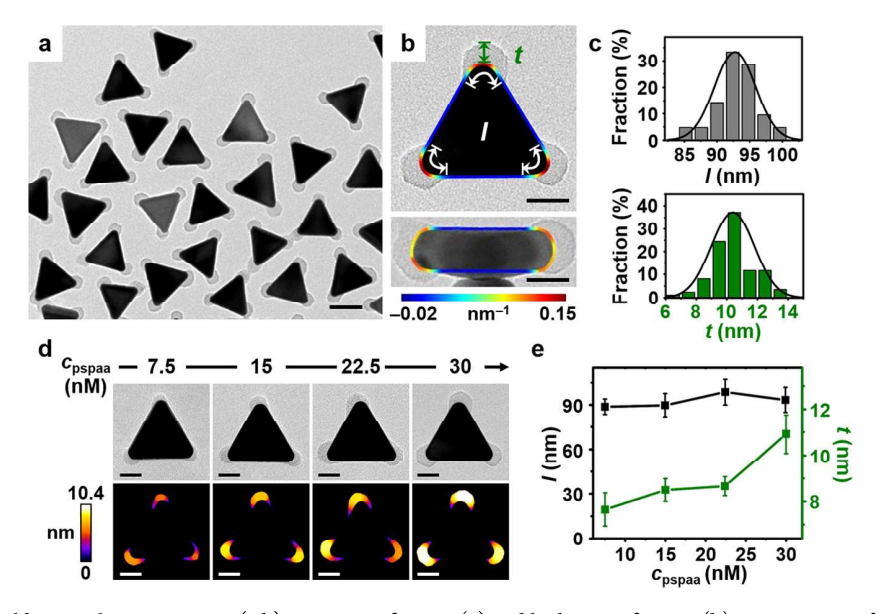


Figure 1. Tip-patched gold triangular nanoprisms. (a,b) Low-magnification (a) and high-magnification (b) TEM images of tip-patched gold prisms, the latter overlaid with prism contours colored to local curvature (Section 6.3 of Supporting Information). (c) Histograms of the cover length l and patch thickness t of the patchy prisms in panel a. (d) Representative TEM images (top) and local thickness analysis (bottom, details in Section 6.2 of Supporting Information) of patchy prisms as c_{pspaa} increases, at a constant α . (e) Plot showing how t and l change with c_{pspaa} . Scale bars: 50 nm (a), 20 nm (b,d).

contrast¹² of PS-b-PAA. The cover length l of the patches along the prism contour and the patch thickness t (labeled in Figure 1b and Figure S3) both have low dispersity of 4% and 13.5%, respectively (Figure 1c). Zoomed-in top and side views of a representative patchy prism, overlaid by the prism's contour colored to local curvature, show that the patches only cover the highly curved tips, leaving the flat basal plane and sides of the prism free of polymer coating (Figure 1b).

The polymer patches are originated from selective 2-NAT adsorption on gold prisms, as PS-b-PAA attaches only where 2-NAT ligands are adsorbed. 20,21 Such site-selective ligand adsorption is consistent with earlier work on tip-functionalization of gold²²⁻²⁵ and CdSe²⁶ nanorods, presumably due to enthalpic preference of ligands to cover the less-coordinated curved tips. 25,27,28 Moreover, simulations suggested that ligands attached to curved surface have more entropic gain than those on flat surface, which depends on the ligand length and structure.²⁹ Indeed, the tip-selectivity of ligand adsorption in our system decreases when we use alkanethiols or flexible polycyclic aromatic hydrocarbons (Figure S4, Section 3.4 of Supporting Information). In comparison, 2-NAT has rigid, conjugated polycyclic aromatic rings of inhibited rotational freedom³⁰ to favor site-selective adsorption on the tips. As a result, when we fix the 2-NAT to prism ratio (α , the ratio of 2-NAT molar concentration to optical density of the prism suspension at its maximum extinction wavelength) and consequently the size of the 2-NAT coated regions, the polymer tip patches keep the same cover length l even upon a 4-fold increase in the PS-*b*-PAA concentration (c_{pspaa}) (Figure 1d,e, Figure S5). The patch thickness t controllably increases, possibly due to more extended conformation³¹ of PS-b-PAA as the packing density on the prism tips increases with higher c_{pspaa}, which was confirmed by the thermal gravimetric analysis (Figure S6). The combination of 2-NAT and PS-b-PAA was used on gold NPs, 20,21 where only uniform polymer coating was observed. We attribute the difference to the 20-50 times higher 2-NAT to NP ratio in those earlier studies than ours,

which can overwhelm the site-selectivity of 2-NAT with too much ligand excess.

Now that the initial 2-NAT adsorption is tip-selective, we increase the 2-NAT concentration to expand the ligand islands, thereby controlling the lateral size of the patches (Table S2 for synthesis details). Both projected TEM images and SCFT modeling validate the hypothesis that ligand island formation leads to the library of patchy prisms we obtain, including small lobed, big lobed, trefoil, T-shape, and reuleaux triangle (Figure 2a-c and Figure S7). As α increases, the tip patches at low α (l= 93.3 nm for α = 0.12 mM) expand laterally over the prism side, first into widened tip patches (l = 113.7 nm for $\alpha = 0.25$ mM; l = 149.7 nm for $\alpha = 1.0$ mM), and then into T-shaped patches with two adjacent patches merged ($\alpha = 2.0 \text{ mM}$). The latter symmetry-breaking is resultant from insufficient α to merge the three tip patches all together. As α increases further, we retrieve the reuleaux triangle patch as reported earlier.1 Raman spectra of three types of 2-NAT coated prisms at increasing α (Figure 2d) confirm a consistent increase of the peak intensities at 1374, 1423, and 1444 cm⁻¹, which correspond to the stretching modes of polycyclic aromatic hydrocarbon ring in 2-NAT, ^{32,33} validating our hypothesis that increased thiol adsorption relates to patch expansion. Furthermore, in SCFT modeling, 34–38 we discern our hypothesized ligand island formation from the alternative possibility of a stochastic Langmuir adsorption on the prism side as α increases (Figures S8 and S9). Specifically, we use a two-dimensional model for the prism with site-specific attraction to the polymer (ϵ_0 for the prism side; ϵ_1 for the prism tip; Section 7 of Supporting Information). We define a coverage parameter $n_{\rm L}(\theta)$ along the side of the prism, where θ is a coordinate along the prism away from the tip that is already covered with 2-NAT. As shown in Figure S9, uniformly increasing ligand adsorption $(n_L(\theta) = n_{L,0} \text{ as a constant})$ leads to encompassing the entire prism as α increases. However, the size of the lobes at intermediate α does not change; rather, more PS-b-PAA adsorbs onto the prism side, which is

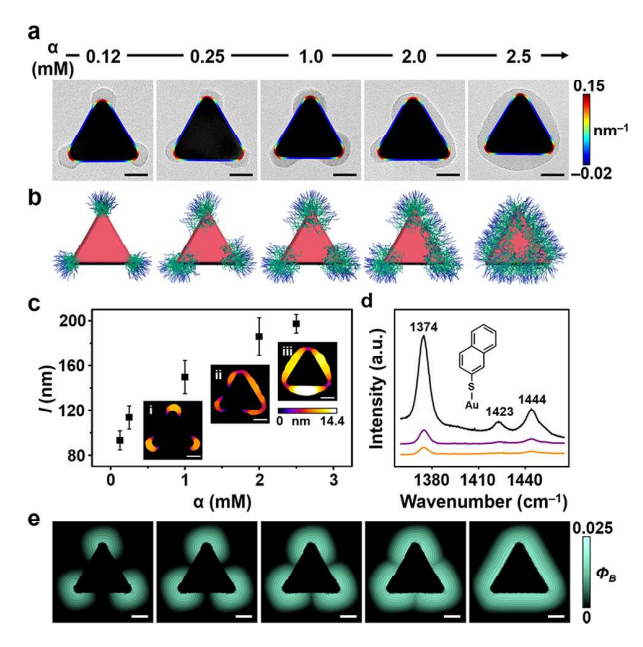


Figure 2. Surface patches from ligand island formation. (a,b) TEM images (a) and schematics (b) of patchy prisms synthesized at varying α . (c) Plot showing increased cover length l with increasing α . Inset: local thickness maps of small lobed (i), T-shaped (ii), and reuleaux triangle (iii) patchy prisms. (d) Raman spectra of gold prisms at α = 0.12 mM (orange), α = 1.0 mM (purple), and α = 5.0 mM (black) (Table S3 for synthesis details). (e) Volume fraction maps of the charged B block, ϕ_B , for patchy prisms obtained from SCFT, where patches are formed from lateral expansion of ligand islands nucleated at the tips. The patch size Λ , is 3, 7, 12, 20, 40 from left to right. Scale bars: 20 nm (a,c,e).

inconsistent with the observed gradual expansion of the lobes to reuleaux triangle (Figure 2a). If we instead use a ligand island formation model $(n_L(\theta) = [1 + (\theta/\Lambda)^{10}]^{-1})$ characterized by an island growth length scale Λ , we see the expected lobe growth along the prism side (Figure 2e), supporting the hypothesis that ligand islands nucleated on the tips expand along the prism side.

The ligand island formation is further elucidated in three dimensions (3D) using atomic force microscopy (AFM), which consistently contrasts with a Langmuir adsorption 39,40 where lateral ligand-ligand interaction is negligible and random adsorption on unoccupied surface occurs regardless of initial ligand sites. As shown in Figure 3a,d,e, the small lobed prism measures a net lobe height (z) of 4.6 nm. The trefoil prism has a higher z of 9.4 nm (Figure 3b,d,f), with lobes expanded into contact along the prism sides. The phase images of the two samples (Figure S10) confirm the uncoated prism regions at the center. Particularly interesting are the reuleaux triangle prisms at the highest α . They resemble a donut shape with a dent at the prism center (Figure 3c,d,g), which again agrees with the island expansion from the prism tips, not from stochastic ligand adsorption.

Lastly, we show that the tip patches on the prisms impact the self-assembly, using the small lobed prisms as an example. They stay dispersed in deionized water due to electrostatic repulsion (ζ -potential: -56 mV). As we increase the ionic strength I to 66.7 mM to screen the electrostatic repulsion between PAA blocks, we obtain two types of unexpected twisted dimeric structures (star, slanting diamond, Figure 4a,e, and Figures S11 and S12). In stars, prisms bring their faces

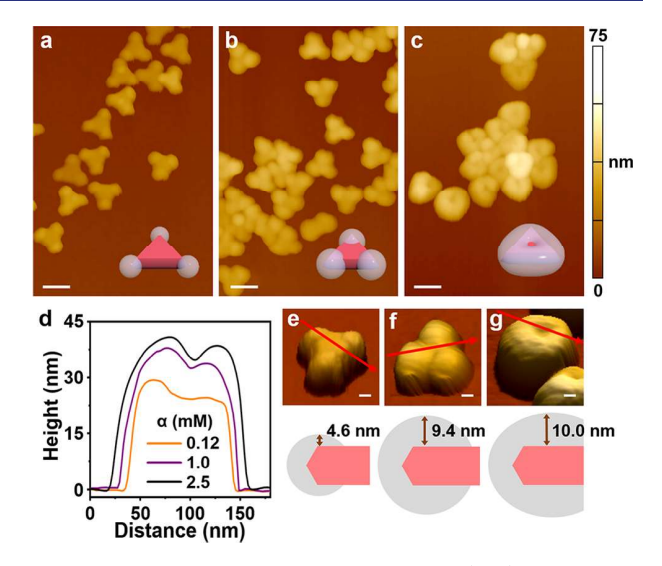


Figure 3. AFM analysis of 3D-shaped patches. (a-c) AFM images and schematics of small lobed, trefoil, and reuleaux triangle patchy prisms. (d) Height analysis on the patchy prisms based on line scans labeled in red arrows in the AFM images (top in e-g) and the corresponding side-view schematics (bottom in panels e-g). Scale bars: 100 nm (a-c), 20 nm (e-g).

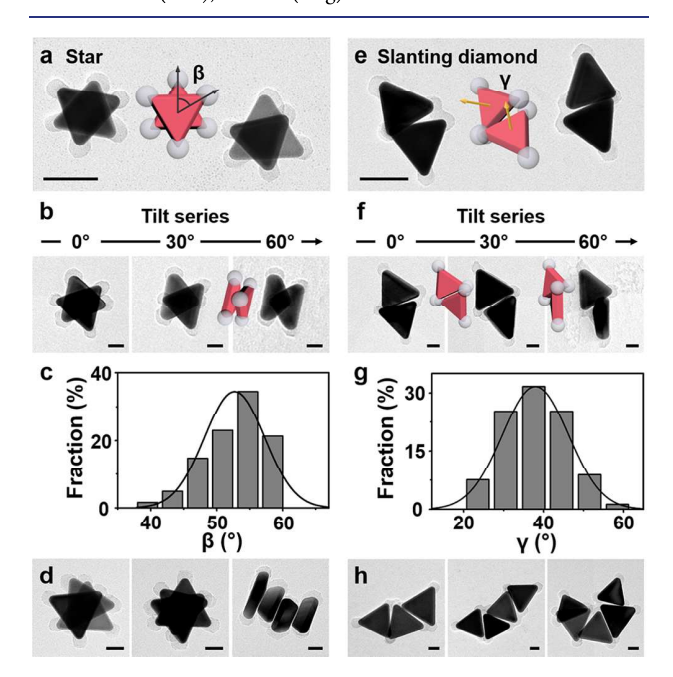


Figure 4. Self-assembly of small lobed prisms into twisted (a-d) star and (e-h) slanting diamond structures. (a,e) TEM images and schematics with angle notation, (b,f) TEM tilt series, (c,g) histogram of misaligned angles, and (d,h) TEM images of the assemblies. Scale bars: 50 nm (a,e), 20 nm (b,d,f,h).

together, and rotate in plane such that patches are distant from one another with a misaligned angle β (Figure 4a,b), whose distribution centers at 52.4° (Figure 4c), likely due to electrostatic repulsion and steric hindrance of the polymer patches. More trimers and tetramers composed of the same motifs are observed at a higher I (80–100 mM) (Figure 4d). In slanting diamonds, prisms bring their sides together, and rotate out of the plane (Figure 4e) such that two patches from each prism overlap, as indicated by the TEM tilt series (Figure 4f, Figure S13). The dihedral angle γ between the two prism planes is $38.7 \pm 8.3^{\circ}$ (Figure 4g, Figure S14, Section 6.4 of Supporting Information), which extends to trimer, tetramer, pentamer, and oligomer (Figure 4h, Figure S15). Yield analysis of self-assembly shows that slanting diamond is the preferred structure and its yield slightly increases at a higher I (Figure \$16). We expect a decrease in the patch size can favor the assembly into stars to maximize the overlap between basal planes, as suggested by previous work on self-assembly of bare prisms.¹⁹ The twisted assemblies are different from those of uniformly coated prisms. ^{19,41} We expect the twisting to bring distinct plasmonic behaviors, ^{42,43} chiral properties, ^{44,45} and large-scale assemblies with high porosity and mechanical strength. 46-48 Considering the stimuli-responsiveness of the patches to solvent polarity, 10,11 pH, 49 and temperature, 12 we foresee a potent library of reconfigurable NPs made by this strategy to adapt to external environment.

ASSOCIATED CONTENT

S Supporting Information

The Supporting Information is available free of charge on the ACS Publications website at DOI: 10.1021/jacs.9b05312.

Detailed descriptions of synthetic protocols, characterization methods, self-assembly, image analysis, and SCFT simulation; additional SEM and TEM images; UV-vis spectra; TGA results; schematic of the SCFT setup and additional SCFT results; AFM phase images; dihedral angle analysis; yield and composition analysis (PDF)

AUTHOR INFORMATION

Corresponding Author

*qchen20@illinois.edu

Shan Zhou: 0000-0002-6476-3280 Charles E. Sing: 0000-0001-7231-2685 Qian Chen: 0000-0002-1968-441X

Author Contributions

 ¶ These authors contributed equally to this work.

Notes

The authors declare no competing financial interest.

ACKNOWLEDGMENTS

This research was supported by the National Science Foundation under Grant No. 1752517. Experiments were carried out in part in the Materials Research Laboratory (MRL) Central Research Facilities, University of Illinois. We thank Dr. Jessica Spear and Dr. Roddel Remy (MRL, University of Illinois) for assistance with AFM and TGA measurements.

REFERENCES

- (1) Vericat, C.; Vela, M. E.; Benitez, G.; Carro, P.; Salvarezza, R. C. Self-Assembled Monolayers of Thiols and Dithiols on Gold: New Challenges for a Well-Known System. Chem. Soc. Rev. 2010, 39, 1805 - 1834
- (2) Poirier, G. E.; Pylant, E. D. The Self-Assembly Mechanism of Alkanethiols on Au(111). Science 1996, 272, 1145-1148.
- (3) Love, J. C.; Estroff, L. A.; Kriebel, J. K.; Nuzzo, R. G.; Whitesides, G. M. Self-Assembled Monolayers of Thiolates on Metals as a Form of Nanotechnology. Chem. Rev. 2005, 105, 1103-1170.

- (4) Doudevski, I.; Schwartz, D. K. Concentration Dependence of Self-Assembled Monolayer Island Nucleation and Growth. J. Am. Chem. Soc. 2001, 123, 6867-6872.
- (5) Chen, T.; Yang, M.; Wang, X.; Tan, L. H.; Chen, H. Controlled Assembly of Eccentrically Encapsulated Gold Nanoparticles. J. Am. Chem. Soc. 2008, 130, 11858-11859.
- (6) Zhu, H.; Fan, Z.; Yu, L.; Wilson, M. A.; Nagaoka, Y.; Eggert, D.; Cao, C.; Liu, Y.; Wei, Z.; Wang, X.; He, J.; Zhao, J.; Li, R.; Wang, Z.; Grünwald, M.; Chen, O. Controlling Nanoparticle Orientations in the Self-Assembly of Patchy Quantum Dot-Gold Heterostructural Nanocrystals. J. Am. Chem. Soc. 2019, 141, 6013-6021.
- (7) Grzelczak, M.; Vermant, J.; Furst, E. M.; Liz-Marzán, L. M. Directed Self-Assembly of Nanoparticles. ACS Nano 2010, 4, 3591-3605.
- (8) Wu, Z.; Li, L.; Liao, T.; Chen, X.; Jiang, W.; Luo, W.; Yang, J.; Sun, Z. Janus Nanoarchitectures: From Structural Design to Catalytic Applications. Nano Today 2018, 22, 62-82.
- (9) Zhang, Y.; Huang, K.; Lin, J.; Huang, P. Janus Nanoparticles in Cancer Diagnosis, Therapy and Theranostics. Biomater. Sci. 2019, 7, 1262-1275.
- (10) Choueiri, R. M.; Galati, E.; Thérien-Aubin, H.; Klinkova, A.; Larin, E. M.; Querejeta-Fernández, A.; Han, L.; Xin, H. L.; Gang, O.; Zhulina, E. B.; Rubinstein, M.; Kumacheva, E. Surface Patterning of Nanoparticles with Polymer Patches. Nature 2016, 538, 79-83.
- (11) Galati, E.; Tebbe, M.; Querejeta-Fernández, A.; Xin, H. L.; Gang, O.; Zhulina, E. B.; Kumacheva, E. Shape-Specific Patterning of Polymer-Functionalized Nanoparticles. ACS Nano 2017, 11, 4995-
- (12) Wang, Z.; He, B.; Xu, G.; Wang, G.; Wang, J.; Feng, Y.; Su, D.; Chen, B.; Li, H.; Wu, Z.; Zhang, H.; Shao, L.; Chen, H. Transformable Masks for Colloidal Nanosynthesis. Nat. Commun.
- (13) Wang, Y.; Zeiri, O.; Neyman, A.; Stellacci, F.; Weinstock, I. A. Nucleation and Island Growth of Alkanethiolate Ligand Domains on Gold Nanoparticles. ACS Nano 2012, 6, 629-640.
- (14) Wang, Y.; Zeiri, O.; Meshi, L.; Stellacci, F.; Weinstock, I. A. Regioselective Placement of Alkanethiolate Domains on Tetrahedral and Octahedral Gold Nanocrystals. Chem. Commun. 2012, 48, 9765-
- (15) Jiang, P.; Nion, A.; Marchenko, A.; Piot, L.; Fichou, D. Rotational Polymorphism in 2-Naphthalenethiol SAMs on Au(111). J. Am. Chem. Soc. 2006, 128, 12390-12391.
- (16) Aravinthan, S.; Cummings, M.; Gould, J.; Haddadi, H.; Mangiacotti, C.; McCabe, K.; Roy, C.; Avila-Bront, L. G. Characterization of Binary Self-Assembled Monolayers Formed from the Sequential Deposition of 2-Naphthalenethiol and Octanethiol. Surf. Sci. 2019, 679, 117-127.
- (17) Wang, Y.; Chen, G.; Yang, M.; Silber, G.; Xing, S.; Tan, L. H.; Wang, F.; Feng, Y.; Liu, X.; Li, S.; Chen, H. A Systems Approach towards the Stoichiometry-Controlled Hetero-Assembly of Nanoparticles. Nat. Commun. 2010, 1, 87.
- (18) Chen, L.; Ji, F.; Xu, Y.; He, L.; Mi, Y.; Bao, F.; Sun, B.; Zhang, X.; Zhang, Q. High-Yield Seedless Synthesis of Triangular Gold Nanoplates through Oxidative Etching. Nano Lett. 2014, 14, 7201-
- (19) Kim, J.; Song, X.; Ji, F.; Luo, B.; Ice, N. F.; Liu, Q.; Zhang, Q.; Chen, Q. Polymorphic Assembly from Beveled Gold Triangular Nanoprisms. Nano Lett. 2017, 17, 3270-3275.
- (20) Chen, G.; Wang, Y.; Tan, L. H.; Yang, M.; Tan, L. S.; Chen, Y.; Chen, H. High-Purity Separation of Gold Nanoparticle Dimers and Trimers. J. Am. Chem. Soc. 2009, 131, 4218-4219.
- (21) Kim, J.; Song, X.; Kim, A.; Luo, B.; Smith, J. W.; Ou, Z.; Wu, Z.; Chen, Q. Reconfigurable Polymer Shells on Shape-Anisotropic Gold Nanoparticle Cores. Macromol. Rapid Commun. 2018, 39, 1800101.
- (22) Huang, Z.; Liu, Y.; Zhang, Q.; Chang, X.; Li, A.; Deng, L.; Yi, C.; Yang, Y.; Khashab, N.; Gong, J.; Nie, Z. Collapsed polymerdirected synthesis of multicomponent coaxial-like nanostructures. Nat. Commun. 2016, 7, 12147.

- (23) Pramod, P.; Thomas, K. G. Plasmon Coupling in Dimers of Au Nanorods. *Adv. Mater.* **2008**, *20*, 4300–4305.
- (24) Zijlstra, P.; Paulo, P. M. R.; Yu, K.; Xu, Q. H.; Orrit, M. Chemical Interface Damping in Single Gold Nanorods and Its near Elimination by Tip-Specific Functionalization. *Angew. Chem., Int. Ed.* **2012**, *51*, 8352–8355.
- (25) Caswell, K. K.; Wilson, J. N.; Bunz, U. H. F.; Murphy, C. J. Preferential End-to-End Assembly of Gold Nanorods by Biotin-Streptavidin Connectors. J. Am. Chem. Soc. 2003, 125, 13914—13915.
- (26) Zhao, N.; Liu, K.; Greener, J.; Nie, Z.; Kumacheva, E. Close-Packed Superlattices of Side-by-Side Assembled Au-Cdse Nanorods. *Nano Lett.* **2009**, *9*, 3077–3081.
- (27) Hinman, J. G.; Eller, J. R.; Lin, W.; Li, J.; Li, J.; Murphy, C. J. Oxidation State of Capping Agent Affects Spatial Reactivity on Gold Nanorods. *J. Am. Chem. Soc.* **2017**, *139*, 9851–9854.
- (28) Indrasekara, A. S. D. S.; Wadams, R. C.; Fabris, L. Ligand Exchange on Gold Nanorods: Going Back to the Future. *Part. Part. Syst. Charact.* **2014**, *31*, 819–838.
- (29) Santos, A.; Millan, J. A.; Glotzer, S. C. Facetted Patchy Particles through Entropy-Driven Patterning of Mixed Ligand SAMS. *Nanoscale* **2012**, *4*, 2640–2650.
- (30) Frey, S.; Stadler, V.; Heister, K.; Eck, W.; Zharnikov, M.; Grunze, M.; Zeysing, B.; Terfort, A. Structure of Thioaromatic Self-Assembled Monolayers on Gold and Silver. *Langmuir* **2001**, *17*, 2408–2415.
- (31) Kim, M.; Schmitt, S. K.; Choi, J. W.; Krutty, J. D.; Gopalan, P. From Self-Assembled Monolayers to Coatings: Advances in the Synthesis and Nanobio Applications of Polymer Brushes. *Polymers* **2015**, *7*, 1346–1378.
- (32) Agarwal, N. R.; Lucotti, A.; Tommasini, M.; Neri, F.; Trusso, S.; Ossi, P. M. SERS Detection and DFT Calculation of 2-Naphthalene Thiol Adsorbed on Ag and Au Probes. *Sens. Actuators, B* **2016**, *237*, 545–555.
- (33) Alvarez-Puebla, R. A.; Dos Santos, D. S.; Aroca, R. F. Surface-Enhanced Raman Scattering for Ultrasensitive Chemical Analysis of 1 and 2-Naphthalenethiols. *Analyst* **2004**, *129*, 1251–1256.
- (34) Fredrickson, G. The Equilibrium Theory of Inhomogeneous Polymers; Oxford University Press, 2005.
- (35) Wang, Q.; Taniguchi, T.; Fredrickson, G. H. Self-Consistent Field Theory of Polyelectrolyte Systems. *J. Phys. Chem. B* **2005**, *109*, 9855–9856.
- (36) Shi, A.-C.; Noolandi, J. Theory of Inhomogeneous Weakly Charged Polyelectrolytes. *Macromol. Theory Simul.* **1999**, *8*, 214–229.
- (37) Jha, P. K.; Zwanikken, J. W.; Detcheverry, F. A.; de Pablo, J. J.; Olvera de la Cruz, M. Study of Volume Phase Transitions in Polymeric Nanogels by Theoretically Informed Coarse-Grained Simulations. *Soft Matter* **2011**, *7*, 5965.
- (38) Nap, R.; Gong, P.; Szleifer, I. Weak Polyelectrolytes Tethered to Surfaces: Effect of Geometry, Acid—base Equilibrium and Electrical Permittivity. *J. Polym. Sci., Part B: Polym. Phys.* **2006**, *44*, 2638–2662.
- (39) Pan, W.; Durning, C. J.; Turro, N. J. Kinetics of Alkanethiol Adsorption on Gold. *Langmuir* **1996**, *12*, 4469–4473.
- (40) Imae, T.; Torii, H. In Situ Investigation of Molecular Adsorption on Au Surface by Surface-Enhanced Infrared Absorption Spectroscopy. *J. Phys. Chem. B* **2000**, *104*, 9218–9224.
- (41) Fu, Q.; Ran, G.; Xu, W. Direct Self-Assembly of CTAB-Capped Au Nanotriangles. *Nano Res.* **2016**, *9*, 3247–3256.
- (42) Kotkowiak, M.; Grześkiewicz, B.; Robak, E.; Wolarz, E. Interaction between Nanoprisms with Different Coupling Strength. *J. Phys. Chem. C* **2015**, *119*, 6195–6203.
- (43) Zhan, P.; Wen, T.; Wang, Z. G.; He, Y.; Shi, J.; Wang, T.; Liu, X.; Lu, G.; Ding, B. DNA Origami Directed Assembly of Gold Bowtie Nanoantennas for Single-Molecule Surface-Enhanced Raman Scattering. *Angew. Chem., Int. Ed.* **2018**, *57*, 2846–2850.
- (44) Greybush, N. J.; Pacheco-Peña, V.; Engheta, N.; Murray, C. B.; Kagan, C. R. Plasmonic Optical and Chiroptical Response of Self-Assembled Au Nanorod Equilateral Trimers. *ACS Nano* **2019**, *13*, 1617–1624.

- (45) Hentschel, M.; Schäferling, M.; Duan, X.; Giessen, H.; Liu, N. Chiral Plasmonics. Sci. Adv. 2017, 3, No. e1602735.
- (46) Walker, D. A.; Leitsch, E. K.; Nap, R. J.; Szleifer, I.; Grzybowski, B. A. Geometric Curvature Controls the Chemical Patchiness and Self-Assembly of Nanoparticles. *Nat. Nanotechnol.* **2013**, *8*, 676–681.
- (47) Miszta, K.; De Graaf, J.; Bertoni, G.; Dorfs, D.; Brescia, R.; Marras, S.; Ceseracciu, L.; Cingolani, R.; Van Roij, R.; Dijkstra, M.; Manna, L. Hierarchical Self-Assembly of Suspended Branched Colloidal Nanocrystals into Superlattice Structures. *Nat. Mater.* **2011**, *10*, 872–876.
- (48) Ceseracciu, L.; Miszta, K.; De Angelis, F.; Marras, S.; Prato, M.; Brescia, R.; Scarpellini, A.; Manna, L. Compression Stiffness of Porous Nanostructures from Self-Assembly of Branched Nanocrystals. *Nanoscale* **2013**, *5*, 681–686.
- (49) Dai, S.; Ravi, P.; Tam, K. C. pH-Responsive Polymers: Synthesis, Properties and Applications. *Soft Matter* **2008**, *4*, 435.